Control system design for concrete irrigation channels

Timm Strecker[1], Michael Cantoni[2] and Ole Morten Aamo[1]

Abstract— **Concrete channels find use at the periphery of irrigation networks, for expansion and to replace small earthen channels given the relative ease of maintenance and elimination of seepage losses. In design, it is important to account for control system performance when dimensioning the channel infrastructure. In this paper, the design of a distributed controller is investigated in terms managing water-levels, and thereby the depth profile (i.e., amount of concrete) needed to support peak flow load under the power of gravity.**

I. INTRODUCTION

Irrigation supports agriculture in many parts of the world. It is estimated that irrigation accounts for approximately 70% of the worldwide water usage [1]. In many situations, water is delivered from reservoirs to farms via a network of open channels under the power of gravity. The flow of water is controlled by adjustable gates located along the channels. Traditionally, such gates have been operated manually, and this is still the case in many parts of the world. Over the last 15-20 years, technologies for automating the operation of irrigation channels have been developed in a collaboration between The University of Melbourne and Rubicon Water, leading to both a significant reduction of water losses and improved quality of service in Northern Victoria, where large-scale installations serving thousands of supply points are currently operational.

Controller design methods for irrigation channels range from PDE-based methods [2], [3], [4], to methods based on simplified integrator-delay models [5], [6], [7], [8]. The latter are usually adopted in practice, because they are more amenable to controller tuning and system identification. Importantly, the simple models approximate the system dynamics very well when operating in closed-loop with relatively slow controllers [9].

To date, the focus of attention has been on large and medium scale channels transporting water from reservoirs to farms. The focus of this paper is on smaller channels at the periphery of distribution network. By virtue of the reduced storage volume in small channels, wave dynamics are more pronounced. This needs to be considered in the controller design.

Within the context of small channels, concrete lining can be employed to eliminate seepage losses and to facilitate maintenance. To avoid spillage and flooding, the water level must remain below the top of the concrete (minus some safety margin) at all times. To manage the required channel depth, and thus the cost of the concrete, achievable control performance should be considered in a co-design of the civil and automation engineering infrastructure. More precisely, controllers should be designed so that water levels do not exceed the height of the concrete at any location along the channel. This is another difference compared to previous work on large-scale channels where this was neglected, as large channels typically have substantial free-board and storage capacity, in order to facilitate manual operation.

The control requirements can be summarized as follows.

1) Regulation of the downstream water level of each section of channel between two gates (within a band of a reference value set by a supervisory control layer) so as to provide quality of service guarantees at the corresponding supply/off-take points.
2) To maintain water-levels along the stretches of channel below specified levels, so as to avoid spillage and flooding, particularly during high flow loads when additional head is required upstream to provide the flow under the power of gravity.
3) String instabilities, i.e., (excessive) amplification of water-level errors and peak flows along the channel, should be avoided.

The paper is organized as follows. In Section II we discuss two types of models for the channel; a high-fidelity PDE model used for analysis and a simpler model used for controller design. The distributed controller structure is also presented there. In Section III some differences relative to larger channels and implications for the design of the decentralized feedback part of the controller are discussed. The design of additional feedfoward compensators, that adjust the downstream water-level reference at each local feedback loop on the basis of downstream flow, are discussed in Section IV in terms of managing the water level profile along the stretch of a channel between the gates. Finally, some concluding remarks are given in Section V.

II. MODELING AND CONTROLLER STRUCTURE

A. Open channel modeling

The section of an irrigation channel between two gates is called a pool. The side view of one such pool is depicted in Figure 1. Water is taken from the channel through outlets which are located at the downstream end of the respective pool. Thus, the flow rate at the downstream end of the pool, Q_{ds}, equals the outflow over the downstream gate plus the sum of the outflows at all outlets. The flow over the gates is

*This work was supported by Statoil ASA, and the Australian Research Council (LP160100666).

[1]Department of Engineering Cybernetics, Norwegian University of Science and Technology (NTNU), Trondheim N-7491, Norway, *timm.strecker@itk.ntnu.no*, *aamo@ntnu.no*

[2]Department of Electrical and Electronic Engineering, The University of Melbourne, Parkville 3010, Australia, *cantoni@unimelb.edu.au*

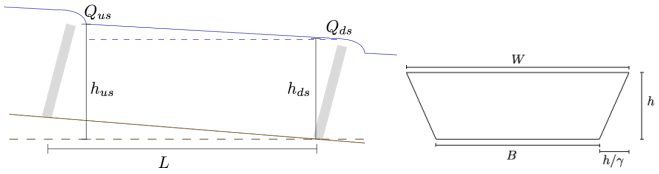

Fig. 1: (Left) Schematic side view of a pool of length L showing the water surface (blue), bottom slope (brown) and overshot gates (grey). The dashed lines depict the horizontal. (Right) Cross-sectional view of a pool with bed width B, water level h, top width W and side slope γ.

controlled via the head over the gate but for simplicity we consider the flow over the gate as the manipulated variable in this paper (which can be related to the head over gate by a static equation). All outflows, and thus Q_{ds}, as well as the downstream water level h_{ds} are measured. Two models for the dynamics in each pool are discussed in the following.

1) Saint Venant equations: The Saint Venant equations are quasilinear hyperbolic PDEs derived from distributed mass and momentum balances which are widely used to model flow in open water channels [10], [11]. They are

$$\frac{\partial A}{\partial t}+\frac{\partial Q}{\partial x}=0 \tag{1}$$

$$\frac{\partial Q}{\partial t}+\left(\frac{gA}{W}-\frac{Q^2}{A^2}\right)\frac{\partial A}{\partial x}+\frac{2Q}{A}\frac{\partial Q}{\partial x}=gA\left(S_0-S_f\right) \tag{2}$$

where t is time and $x\in[0,L]$ is the location measured from the upstream end in a pool of length L, $A(x,t)$ is the wetted cross-sectional area, $Q(x,t)$ is the volumetric flow rate, g the gravitational acceleration, W the channel width (the relation between A, h and W can be derived from the trapezoidal cross-section geometry, see Figure 1), S_0 is the bottom slope and the friction slope is

$$S_f=\frac{n^2Q^2}{A^2R^{4/3}} \tag{3}$$

with Manning coefficient n and hydraulic radius R. Note that A, Q and S_f are functions of (x,t) and the parameters may potentially vary with x, but we omit the arguments in (1)-(2) for brevity.

We use (1)-(2) as a high-fidelity reference model to verify the controller design.

2) Integrator and delay model: For the controller design, we use the following simplified model (see also [9])

$$\dot{h}_{ds}(t)=\frac{1}{\alpha}\left(Q_{in}(t-\tau)-Q_{out}(t)\right), \tag{4}$$

where $\alpha=LW$ is the water surface area and τ is the delay in the pool (i.e. L divided by the wave propagation speed (≈ 3 m/s)). That is, downstream outflow decreases the downstream water level by emptying the pool while upstream inflow fills the pool and thus, after a delay, increases the downstream water level. Note that (4) is not capable of modeling waves in the pool, but the model is relatively accurate if wave dynamics are not excited.

3) Coupling conditions: The models (1)-(2) and (4) represent the dynamics of one pool. For a channel consisting of N pools, let the superscript ^{i} denote the pool number such that the 1-st pool is the most upstream pool and the N-th pool is the most downstream one. Let Q^i_{out} denote the outtake at the outlet located at the downstream end of the i-th pool. Then, the coupling conditions between neighboring pools are

$$Q^N(L^N,t)=Q^N_{ds}=Q^N_{out}(t) \tag{5}$$

$$\vdots$$

$$Q^i(L^i,t)=Q^i_{ds}=Q^{i+1}_{in}(t)+Q^i_{out}(t) \tag{6}$$

$$\vdots$$

$$Q^1(L^1,t)=Q^1_{ds}=Q^2_{in}(t)+Q^1_{out}(t) \tag{7}$$

where the upstream inflow into the i-th pool, Q^i_{in}, is determined by the i-th controller. Note that there are no boundary conditions on the water levels which are determined by the inflows and outflows and the initial condition.

	pool 1	pool 2	pool 3	pool 4
L	200m	900m	300m	700m
B	0.75m	0.75m	0.75m	0.75m
γ	3.2	3.2	3.2	3.2
n	0.012	0.012	0.012	0.012
h_{ref}	1m	1m	1m	1m
S_0	0.0002	0.0002	0.0002	0.0002
τ	1.1min	5min	1.7min	3.9min
K_p	0.96	0.83	0.92	0.85
T_i	19min	100min	30min	76min,
T_f	2.2min	10min	3.3min	7.8min

TABLE I: Channel and controller parameters. Pools are numbered from upstream to downstream.

4) Exemplary channel: The parameters of an exemplary channel consisting of 4 pools are given in Table I where the controller parameters K_p, T_i and T_f will be introduced in Section III. We use these parameters if not stated otherwise.

B. Controller structure

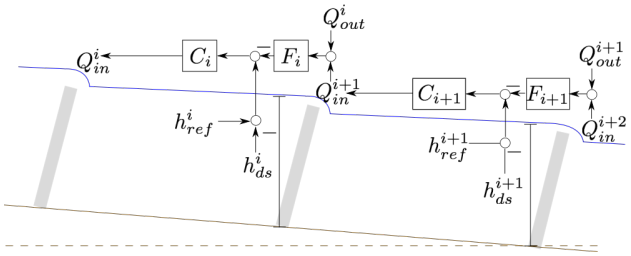

Fig. 2: Controller structure.

In this paper we consider the distributed distant-downstream control architecture depicted in Figure 2, where the inflow over the upstream gate is used to control the downstream water level to a reference value by the feedback controller C_i. The downstream water-level reference is set by a supervisory controller based on the predicted/scheduled load and is assumed to be a given constant in this paper.

The distant-downstream control architecture has the merit that water is released from upstream reservoirs on demand, whereas a drawback of this strategy is that the transport delay in the pools limits achievable closed-loop performance [7]. The water-level profile as well as the closed-loop dynamics can be improved by the feedforward paths F_i in Figure 2. The design of the feedforward gains F_i is discussed further in Section IV.

III. Feedback Controller

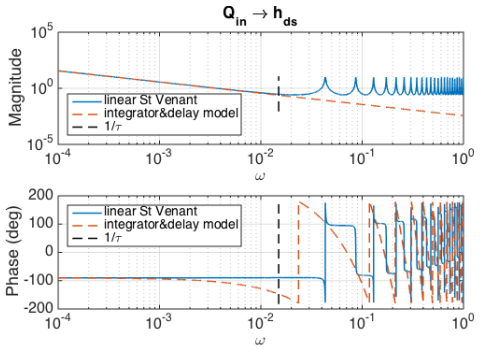

Fig. 3: Bode plot of the transfer function from Q_{in} to h_{ds} for pool 1 in table I with $Q_0 = 5ML/d$ and $h_{ref} = 1\,\text{m}$.

Motivated by its simplicity the feedback controller design is based on the simplified integrator & delay model (4). However, (4) is not capable of modeling wave dynamics that occur at high frequencies and the St Venant model (1)-(2) is more reliable in this regard. The transfer functions from upstream inflow to donwstream water level in a small pool which can be derived by Laplace-transforming (4) and the linearization of (1)-(2) around a nominal flow rate Q_0 and water level profile as determined by h_{ref}, respectively, are compared in Figure 3. The integrator & delay model is a good approximation for frequencies slower than approximately $1/\tau$ where τ is the delay in the pool. At higher frequencies, however, the pool does not act like an integrator but standing waves are created. Because of the small storage volume and the relatively small friction factor, these resonances are significant, much more than in the larger pool in Figure 4 which is typical for a secondary channel.
Following [8] we use for the feedback controller a PI controller with roll-off of the form

$$C(s) = K_p \frac{T_i s + 1}{T_i s (T_f s + 1)} \tag{8}$$

where the purpose of the roll-off term $1/(T_f s + 1)$ is to reduce the controller gain at high frequencies where there is a significant mismatch between the integrator & delay model and the actual dynamics. The controller parameters used for the exemplary channel, which can be obtained by standard loop-shaping techniques, are given in Table I. The Nyquist plot for the smallest pool in the channel in closed loop with C for different roll-off parameters T_f is shown in Figure 5. Since both the open-loop system and the controllers have no unstable poles or zeros, the closed-loop system is stable if the Nyquist curve does not encircle $(-1,0)$. For $T_f = 0.7\tau$, for instance, the integrator & delay model suggests a significant robustness margin for the closed-loop system but the system is unstable according to the linearized St Venant model. $T_f = \tau$ ensures closed-loop stability but the robustness margin is tiny, while $T_f = 2\tau$ ensures stability and some degree of robustness. The encirclement of $(-1,0)$ occurs at high frequencies that are hardly excited in practice, but instability should be avoided nevertheless. For the larger pool in Figure 4 the Nyquist plots when using the integrator & delay and St Venant models are almost identical for any T_f unless C has unreasonably high gain at high frequencies.

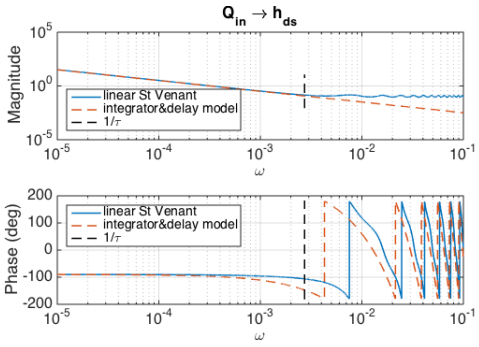

L	B	S_0	γ	n	h_{ref}	Q_0
1100 m	1.8 m	0.0001	2	0.022	1 m	20 ML/d

Fig. 4: Bode plot of the transfer function from Q_{in} to h_{ds} for a pool in a larger channel with parameters given in the table.

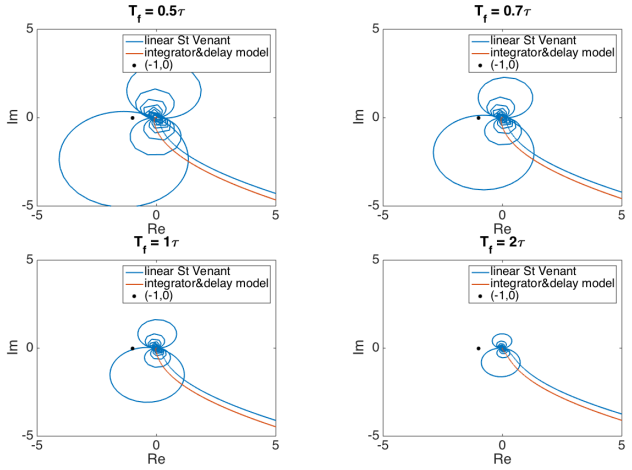

Fig. 5: Nyquist plots for different choices of T_f.

IV. Feedforward Controller Design

As mentioned earlier we base the feedforward controller design on the simpler integrator & delay model. Following the approach in [12], [13] we design the feedforward term F on a pool-by-pool basis such that the closed-loop transfer function from downstream outflow Q_{ds} to upstream inflow

Q_{in} becomes a desired transfer function which we denote by G. It can be shown that

$$G(s) = C(s)\left(1 + \frac{1}{\alpha s} e^{-s\tau} C(s)\right)^{-1} \left(\frac{1}{\alpha s} - F(s)\right) \quad (9)$$

where the case with pure feedback corresponds to $F = 0$. For a given desired G, (9) can be solved for F which gives

$$F = \frac{1}{\alpha s}\left(1 - G(s)e^{-s\tau}\right) - \frac{G(s)}{C(s)}. \quad (10)$$

As C has relative degree 1 (see (8)), G must have relative degree at least 1 to ensure that F is proper. It is reasonable to restrict the quest for a desirable G to LTI systems which we write without loss of generality in the form

$$G(s) = \frac{1 + b\tau s + \ldots}{1 + a\tau s + \ldots}. \quad (11)$$

For such G it can be shown (similarly as in [13], page 42) that the steady-state offset Δh_F of the downstream water level due to feedforward for a downstream outflow Q_{ds} is

$$\Delta h_F = \frac{(1 + a - b)\,\tau}{\alpha} Q_{ds} = \frac{1 + a - b}{cW} Q_{ds}, \quad (12)$$

where $c \approx 3$ m/s is the transport speed and W is the pool width. Thus, the water level offset increases with decreasing pool width, and increases linearly with the outflow.

In the following, we discuss the design of G. The simplest choice would be a low-pass filter

$$G(s) = \frac{1}{1 + a\tau s} \quad (13)$$

which has a as degree of freedom. Note that this choice ensures $\|G\|_{H_\infty} \leq 1$ such that string instability is avoided [12]. Taking $a \lesssim 1$ results in high gain in F at high frequencies which is undesirable due to the mismatch between the linearized St Venant equations and the integrator & delay model at high frequencies as discussed in Section III and because the wave dynamics in the channel are excited. Taking $a \gtrsim 3$ avoids high gain in F at high frequencies but the water-level offset Δh_F as given in (12) becomes excessively large. For instance, taking the pool as in Figure 3, $a = 3$ and a flow rate $Q_{ds} = 30$ML/d results in $\Delta h_F \approx 0.35$ m. Therefore, using a low-pass filter for G is not the optimal choice in small channels.

A second-order transfer function of the form

$$G(s) = \frac{1 + b\tau s}{(1 + \bar{a}\tau s)^2} = \frac{1 + b\tau s}{1 + 2\bar{a}\tau s + (\bar{a}\tau s)^2} \quad (14)$$

has the additional degree of freedom b that can be used to manage Δh_F. In the following we discuss two particular choices for Δh_F. The pure feedback controller achieves tracking of the downstream water-level reference h_{ref} at steady state. For G as in (14), the same is achieved by use of $b = 2\bar{a} + 1$, i.e.

$$G(s) = \frac{1 + (2\bar{a} + 1)\tau s}{(1 + \bar{a}\tau s)^2}. \quad (15)$$

Second, we design G to prevent a steady-state water level increase at the downstream end of the pools during flow loads. The water-level increase at the upstream end of the pools in the channel with parameters as given in Table I is depicted in Figure 6. As described in the introduction an increase in the upstream water level is undesirable because it increases the necessary height of the concrete lining. As illustrated in Figure 7, the water-level increase due to friction can be compensated by lowering the downstream water level reference. For a given anticipated maximum flow rate Q_{max} and given maximum steady-state upstream water level, the required downstream water-level reference can be obtained by solving the steady-state St Venant equations (i.e. (1)-(2) with the time-derivatives set to zero) with the upstream water level set to the maximum water level as boundary condition. Let Δh_f denote the corresponding change in the downstream water level reference. Setting Δh_F at flow rate $Q_{ds} = Q_{max}$ as given by (12) to Δh_f and solving for b gives

$$b = 1 + 2\bar{a} - \frac{\alpha}{Q_{max}\tau}\Delta h_f. \quad (16)$$

The corresponding G is

$$G(s) = \frac{\left((1 + 2\bar{a})\tau - \frac{\alpha}{Q_{max}}\Delta h_f\right)s + 1}{(\bar{a}\tau s + 1)^2}. \quad (17)$$

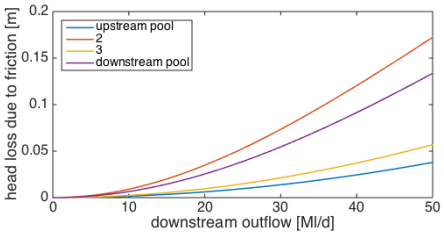

Fig. 6: Water level change due to friction as a function of the flow rate.

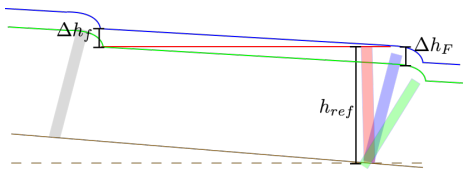

Fig. 7: Water-level profile at zero flow (red), when controlling the downstream water level to h_{ref} (blue) and when lowering the downstream water-level reference by feed-forward to compensate the frictional water-level offset Δh_f (green).

A. Example with small outflows

In the following we use the channel parameters as given in Table I. One outlet is located at the downstream end of each pool. The nonlinear St Venant equations (1)-(2) are simulated in closed loop with the feedback controller and different variants of feedforward. First, we consider an example with relatively small outflows as given in Figure 8a. The resulting time series of the water levels and upstream flow rates for a pure feedback controller (i.e. $F = 0$) is depicted in

Figure 9. The step changes in the outflows cause water-level deviations of approximately 8 cm during transients. Since the cummulative flow load is relatively small even in the most upstream pool, the frictional head loss is small and the upstream water level increases only marginally. The trajectories for the system with feedforward with F as in (10) for G as in (15) are depicted in Figure 10. We use $\bar{a} = 3$ which is sufficiently large to prevent the excitation of high-frequency dynamics while choosing $\bar{a} > 3$ would make the transients unnecessarily slow. That is, the feedforward is such that there is no change to the downstream water level reference at steady state. However, the transients are improved significantly compared to pure feedback. Since friction is small in this example, using feedforward for G as in (17) results in very similar trajectories as using G as in (15).

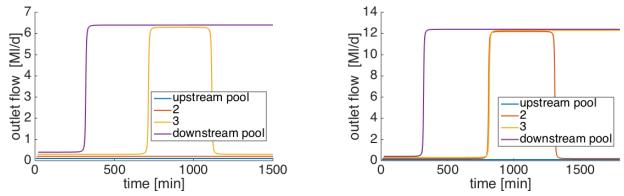

Fig. 8: Outflow through the outlets at the downstream ends of the pools for (a) the small-outflow example and (b) the large-outflow example.

B. Example with large outflows

The trajectories for an example with large outflows as given in Figure 8b are depicted in Figures 11-12. The three most downstream outlets are consecutively opened to 12 ML/d such that the maximum flow load in the two most upstream pools is 36 ML/d. Without feedforward, there are significant deviations of the water levels and flow rate during transients. Moreover, high friction results at in significant increase of approximately 12 cm of the steady-state upstream water level in pool 2 during maximum flow load. In pool 2, the concrete lining would have to be almost 20 cm higher than the reference water level to avoid spilling. By use of feedforward for G as in (17) where Δh_f is computed for $Q_{max} = 36$ ML/d, the transients are much less severe and faster, and the water level increase compared to the reference is negligible at all locations in the channel. This comes at the cost of reducing the downstream water level in pool 2 by almost 20 cm. Using G as in (15) the transients look similar to those in Figure 12 but the steady states are the same as in Figure 11. Of course it is possible to choose G in between the extreme cases (15) and (17) such that there is a moderate water level decrease downstream and a moderate water level increase upstream.

C. String stability

String instability can cause undesirable water-level fluctuations in a channel. String instability can be excluded if the H_∞-norm of the closed-loop transfer function from Q_{ds} to Q_{in} in each pool is 1 [12]. Due to page restrictions we cannot go into the detail here but it can be said that the feedforward designs using both (15) and (17) result in an H_∞-norm only slightly larger than 1. Due to the small number of pools the resulting water-level overshoots are very small which can also be seen in Figures 10 and 12. In fact, string-instability-induced overshoots are reduced compared to the case without feedforward. Even in a worst-case example with 5 identical pools no significant string-instabilities occurred (not depicted here).

V. Conclusions

In this paper we discussed the control system design for concrete irrigation channels. Waves resonances are more significant than in larger channels. Therefore, the Saint Venant Equations should be used as a high-fidelity model to verify the controller design. One of the main control objectives was to prevent a significant increase of the water level at all locations along the channel during operation in order to keep the required height of the concrete lining minimal. The discussed feedforward scheme adjusting the downstream water level reference depending on the flow load reduces water-level variations during transient. Moreover, the feedforward controller can be tuned to lower the downstream water level such that the friction-induced water level increase in the upstream part of the pools during high flow loads is compensated. By use of this design, string instability problems which had been observed in channels consisting of a much larger number of pools did not occur.

References

[1] Unesco, *The United Nations world water development report*, 2016.

[2] J. de Halleux, C. Prieur, J.-M. Coron, B. d'Andréa Novel, and G. Bastin, "Boundary feedback control in networks of open channels," *Automatica*, vol. 39, no. 8, pp. 1365–1376, 2003.

[3] G. Bastin, J.-M. Coron, B. d'Andrea Novel, and L. Moens, "Boundary control for exact cancellation of boundary disturbances in hyperbolic systems of conservation laws," in *Proceedings of the 44th IEEE Conference on Decision and Control*. IEEE, 2005, pp. 1086–1089.

[4] V. Dos Santos and C. Prieur, "Boundary control of open channels with numerical and experimental validations," *IEEE Transactions on Control Systems Technology*, vol. 16, no. 6, pp. 1252–1264, 2008.

[5] X. Litrico and V. Fromion, "Simplified modeling of irrigation canals for controller design," *Journal of irrigation and drainage engineering*, vol. 130, no. 5, pp. 373–383, 2004.

[6] I. Mareels, E. Weyer, S. K. Ooi, M. Cantoni, Y. Li, and G. Nair, "Systems engineering for irrigation systems: Successes and challenges," *Annual reviews in control*, vol. 29, no. 2, pp. 191–204, 2005.

[7] M. Cantoni, E. Weyer, Y. Li, S. K. Ooi, I. Mareels, and M. Ryan, "Control of large-scale irrigation networks," *Proceedings of the IEEE*, vol. 95, no. 1, pp. 75–91, 2007.

[8] E. Weyer, "Control of irrigation channels," *IEEE Transactions on Control Systems Technology*, vol. 16, no. 4, pp. 664–675, 2008.

[9] ——, "System identification of an open water channel," *Control engineering practice*, vol. 9, no. 12, pp. 1289–1299, 2001.

[10] M. H. Chaudhry, *Open-channel flow*. Springer, 2007.

[11] X. Litrico and V. Fromion, *Modeling and control of hydrosystems*. Springer Science & Business Media, 2009.

[12] L. Soltanian and M. Cantoni, "Decentralized string-stability analysis for heterogeneous cascades subject to load-matching requirements," *Multidimensional Systems and Signal Processing*, vol. 26, no. 4, pp. 985–999, 2015.

[13] L. Soltanian, "Distributed distant-downstream controller design for large-scale irrigation channels," Ph.D. dissertation, The University of Melbourne, 2014.

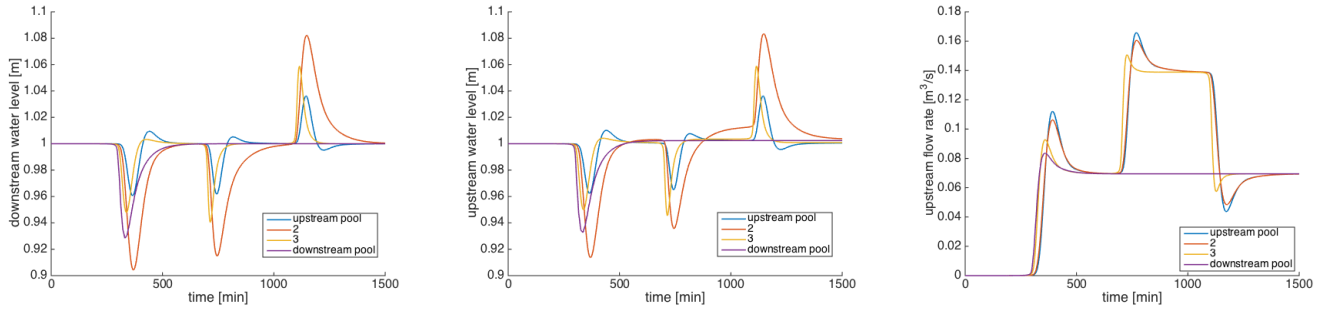

Fig. 9: Trajectories for the small-outflows example without feedforward.

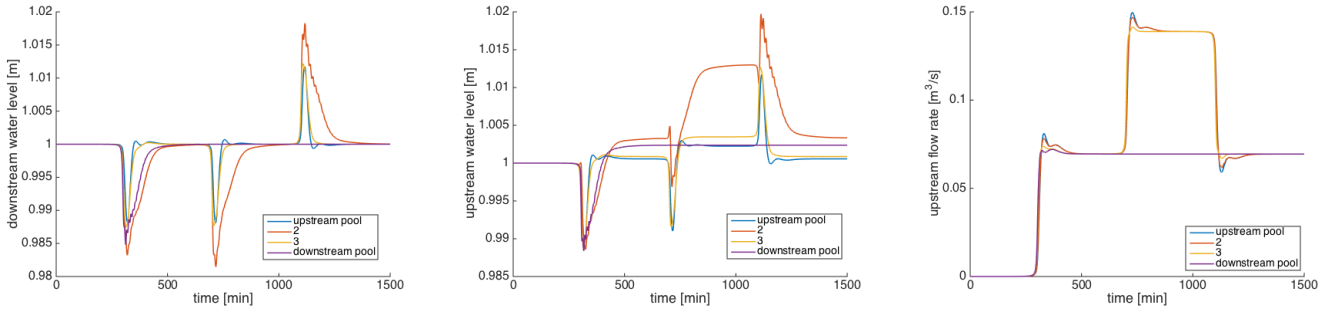

Fig. 10: Trajectories for the small-outflows example with feedforward using F as in (10) with (15) and $\bar{a} = 3$.

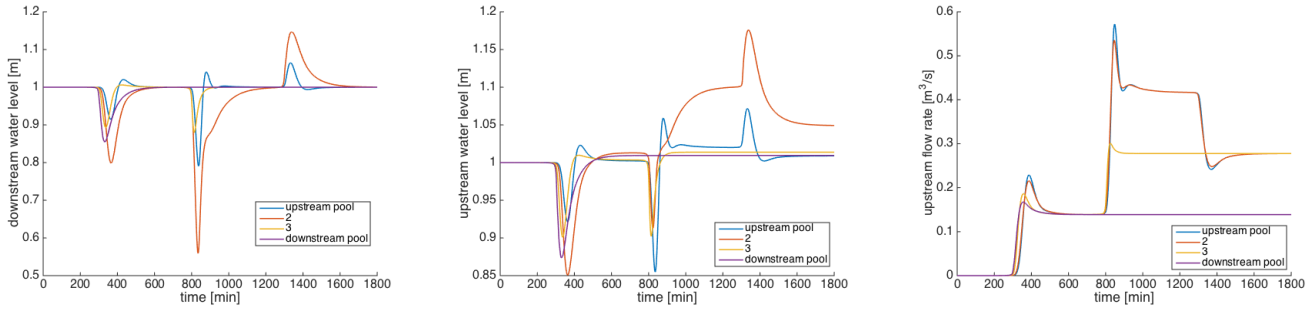

Fig. 11: Trajectories for the small-outflows example without feedforward.

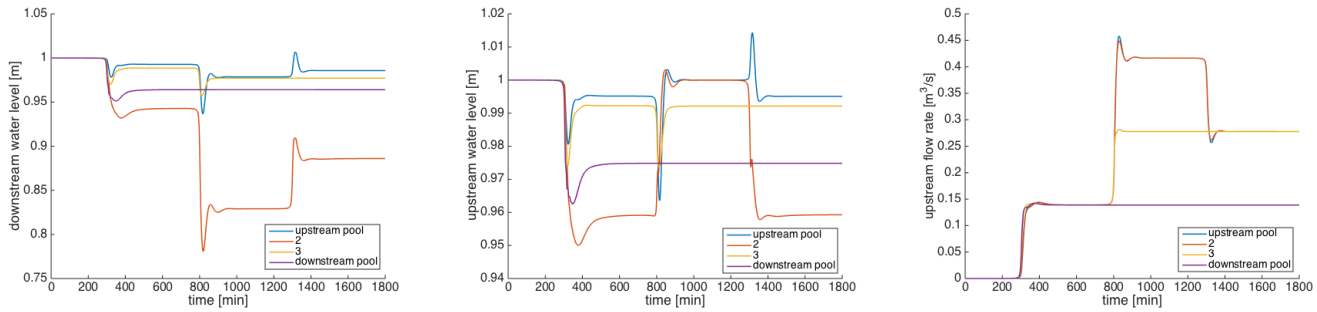

Fig. 12: Trajectories for the small-outflows example with feedforward using F as in (10) with (17) and $\bar{a} = 3$.